| radio | microwave | IR | Visible | UV | X-ray | $\gamma$-ray |
|---|---|---|---|---|---|---|
| $1–10^{9}$ | $10^{9}–10^{12}$ | $10^{12}–4\times10^{14}$ | | $8\times10^{14}–10^{17}$ | $10^{17}–10^{20}$ | $10^{20}$ up |

**Figure 1.1** The electromagnetic spectrum divided into regimes and frequencies within these regimes. Frequency is in units of Hz (i.e., cycles/s).

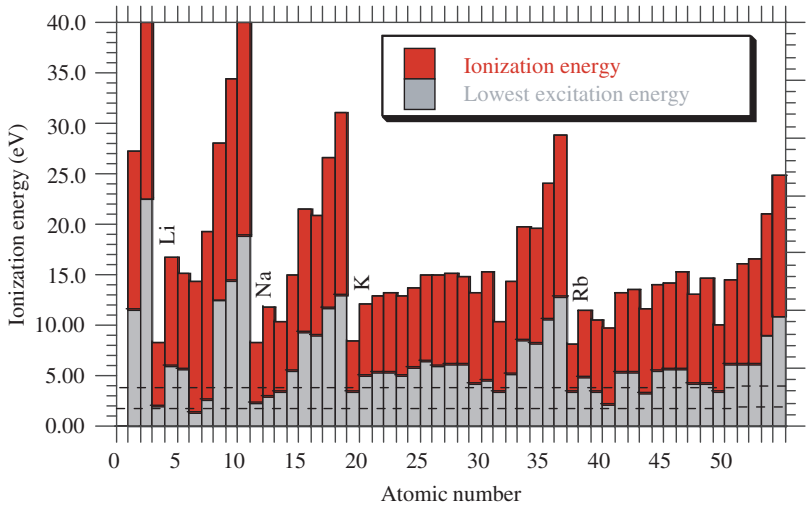


**Figure 2.3** Lowest electronic excitation energy and the ionization energy of the first 50 atoms in the periodic table. The visible region of the spectrum is indicated by the dashed lines. [See replacement file in "errors".]

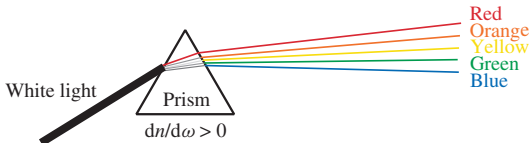


**Figure 2.8** Dispersion of white light by a glass prism.

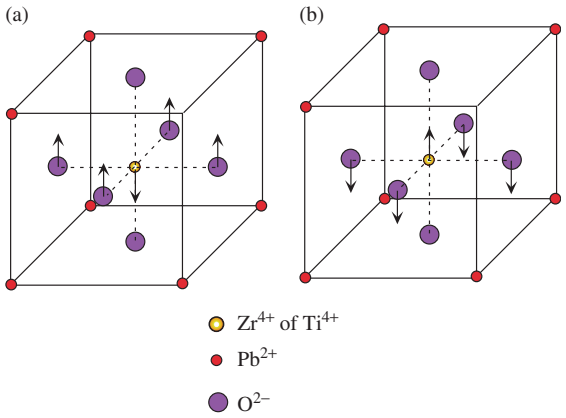


**Figure 2.34** Unit cell of the cubic perovskite Pb $(Zr_xTi_{1-x})O_3$ crystal, with polarization (a) up or (b) down.

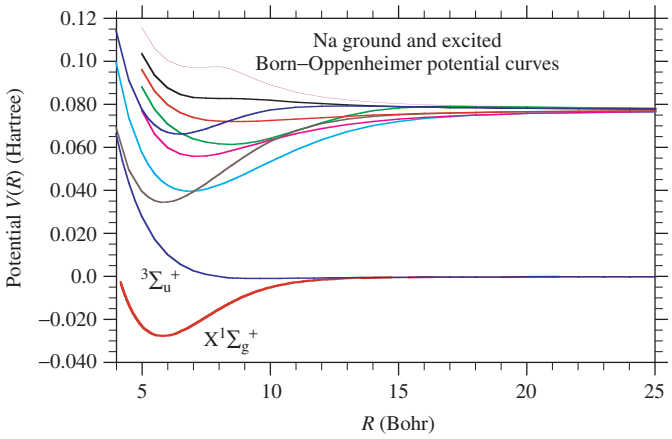


**Figure 3.6** All the adiabatic Born–Oppenheimer ground and excited molecular potential energy curves of sodium.

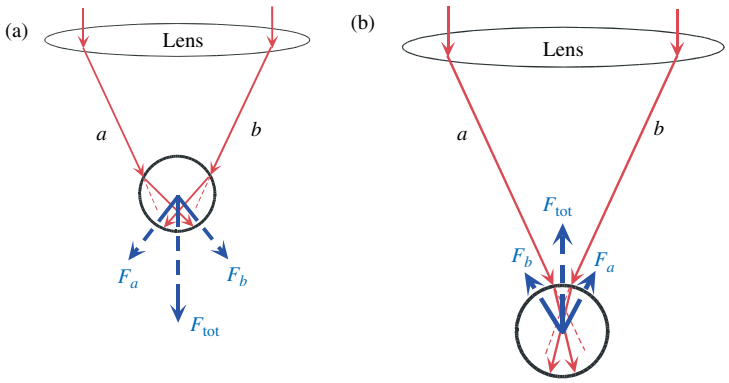


**Figure 3.14** Refraction of a light beam giving rise to optical tweezers. (a) Focus below the object center. (b) Focus above the object center.

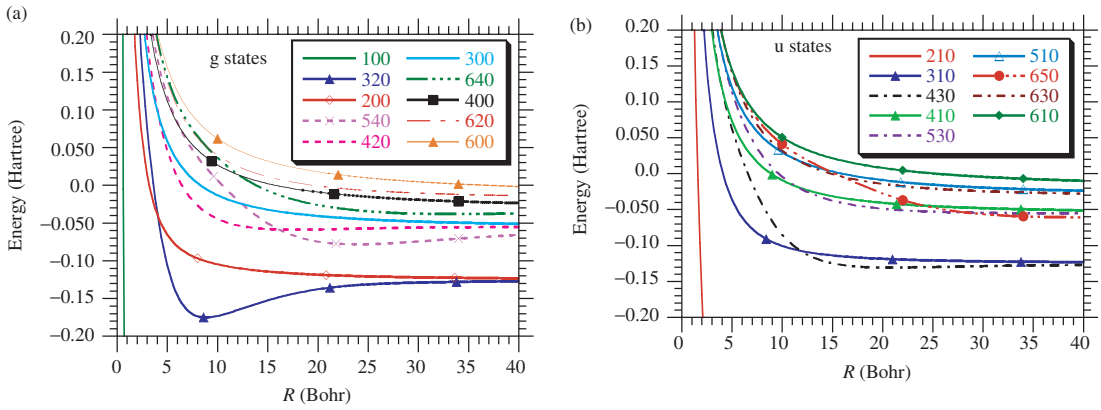


**Figure 6.8** $H_2^+$ excited potential curves for as a function of internuclear distance $R$. Gerade (g) states and ungerade (u) states. The states are labelled by their united atom quantum numbers $nl\lambda$ (see Section 6.3.5).

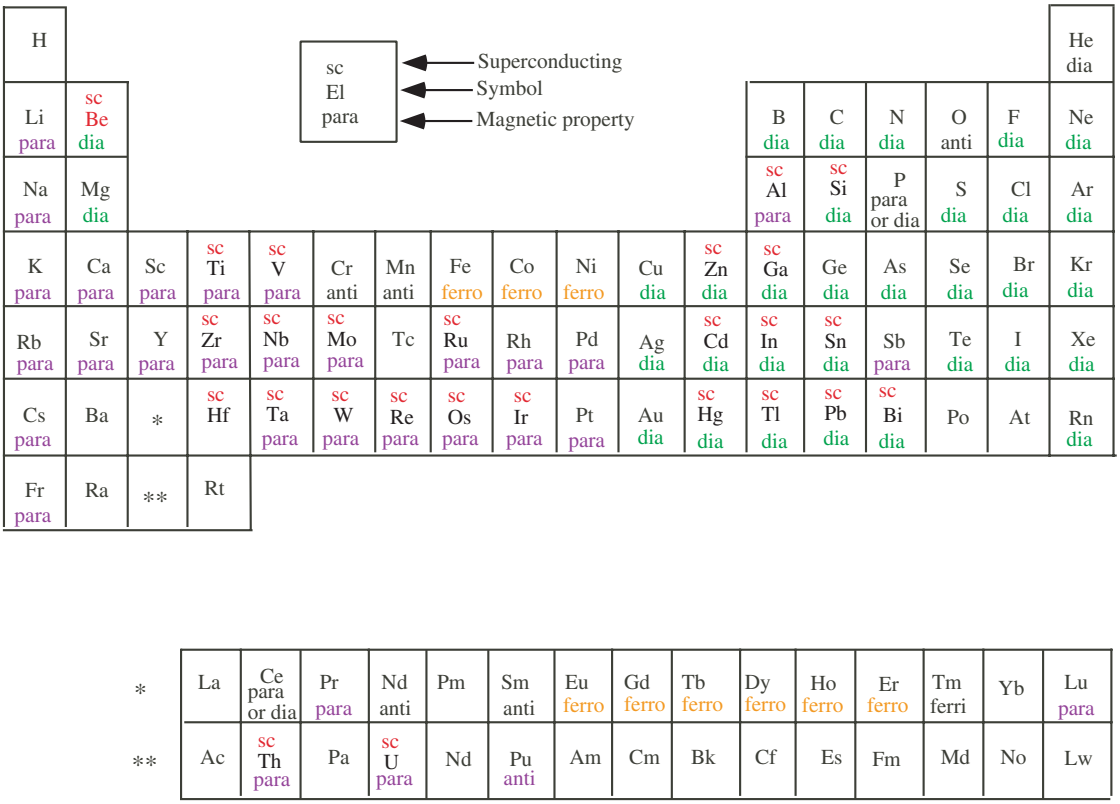


**Figure 4.2** Magnetic properties of the elements at low temperatures.

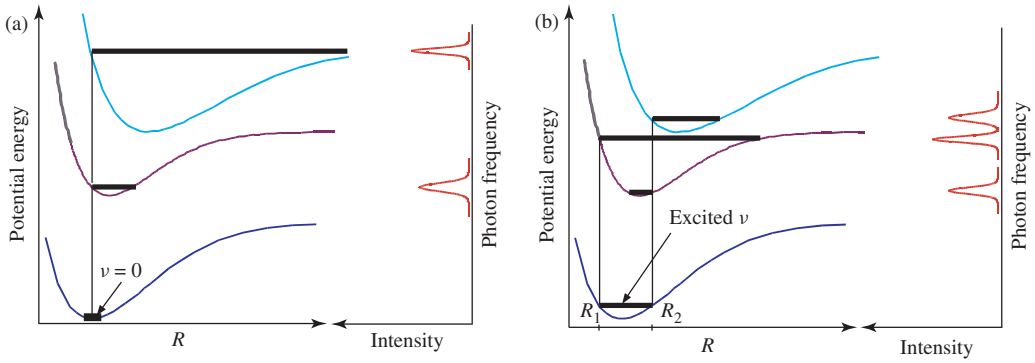


**Figure 6.12** Schematic illustration of the Franck–Condon principle. (a) Absorption from the ground vibrational state of the ground electronic potential. (b) Absorption from an excited vibrational state of the ground electronic potential. The points labelled $R_1$ and $R_2$ are the turning points of the excited vibrational state on the ground electronic potential.

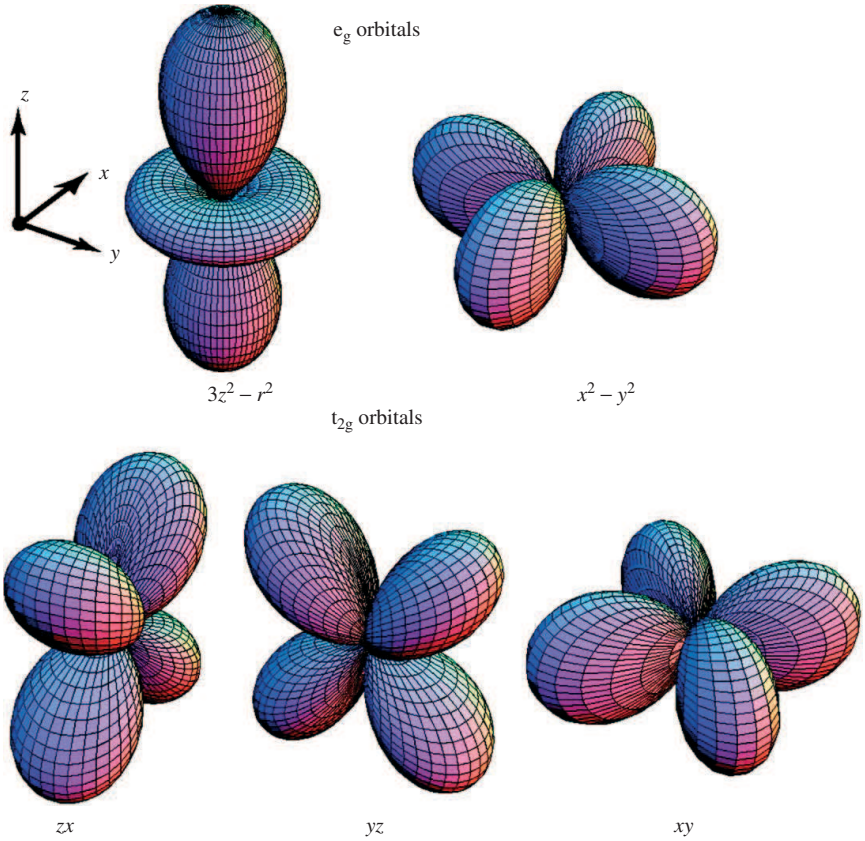


**Figure 6.22** The five d orbital functions.

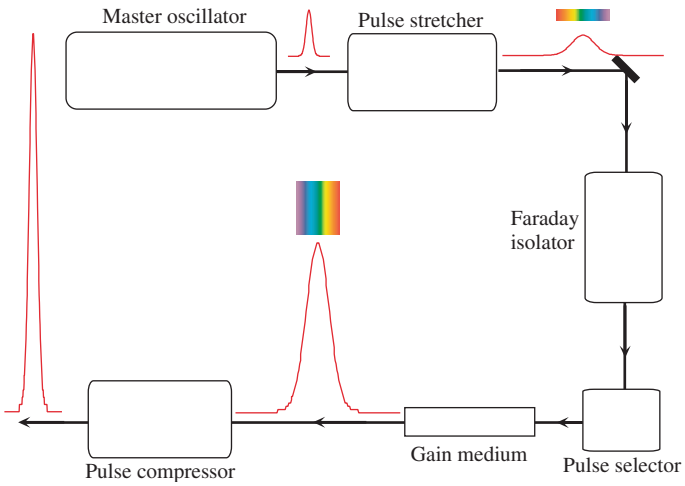


**Figure 7.10** Chirped pulse amplifier system.

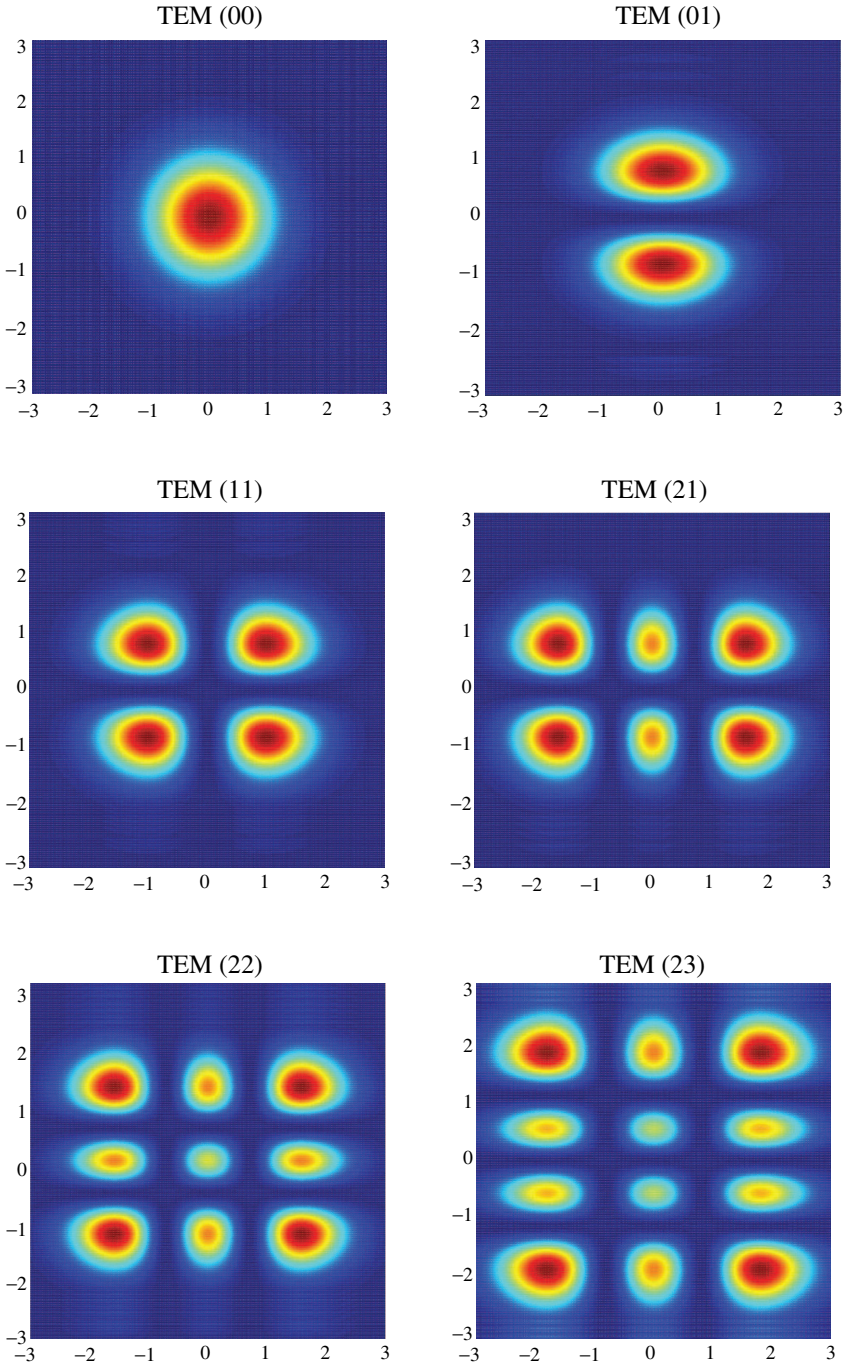


**Figure 7.12** Transverse Hermite−gaussian spatial intensity profiles.

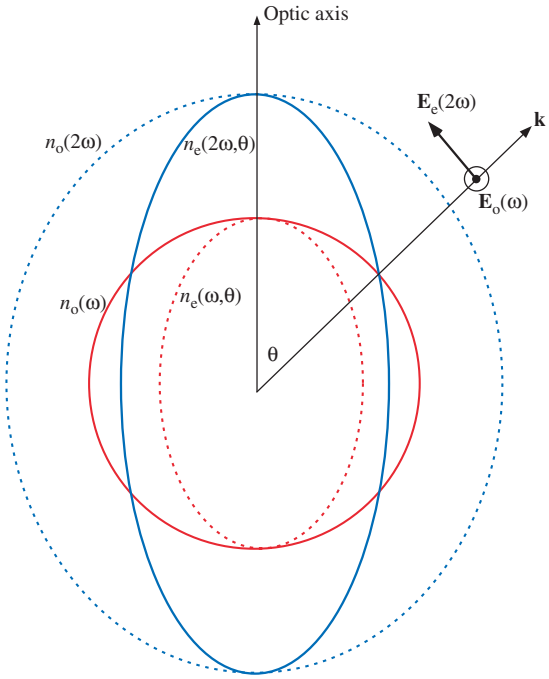


**Figure 8.1** Indices of refraction for the fundamental and the second harmonic in a negative uniaxial crystal ($n_o > n_e$) with type I phase-matching.

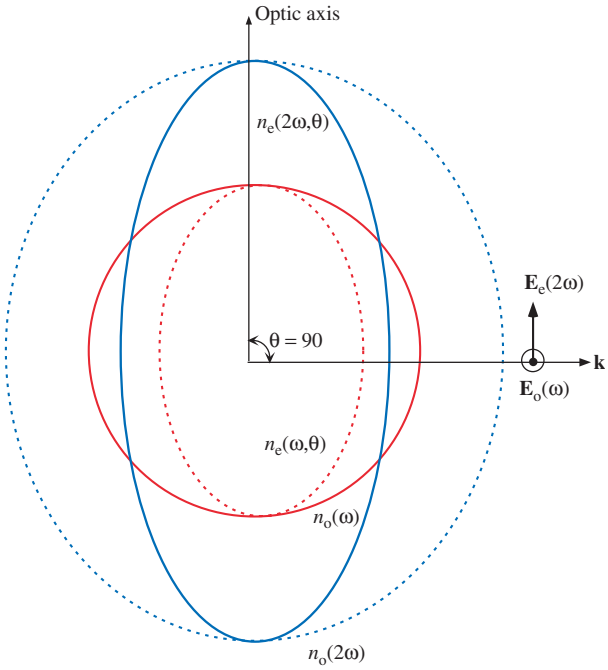


**Figure 8.2** Type I phase-matching with 90° matching.

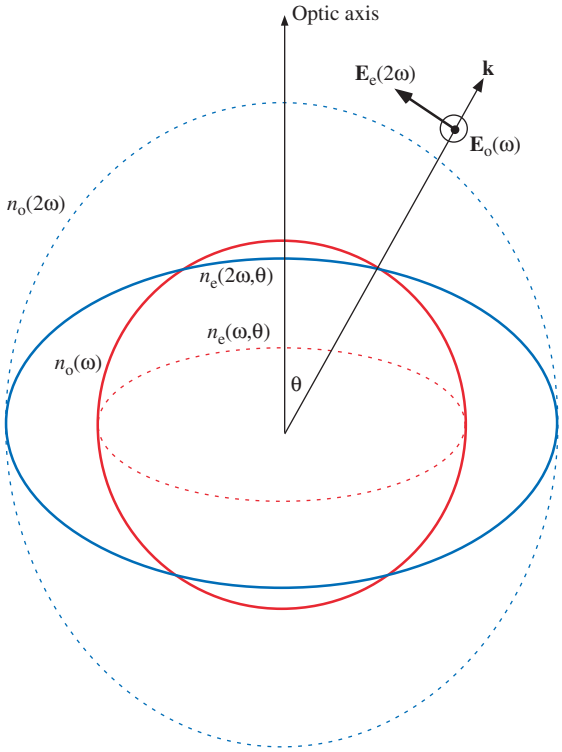


**Figure 8.3** Indices of refraction for the fundamental and the second harmonic in a positive uniaxial crystal ($n_e > n_o$) with type I phase-matching.

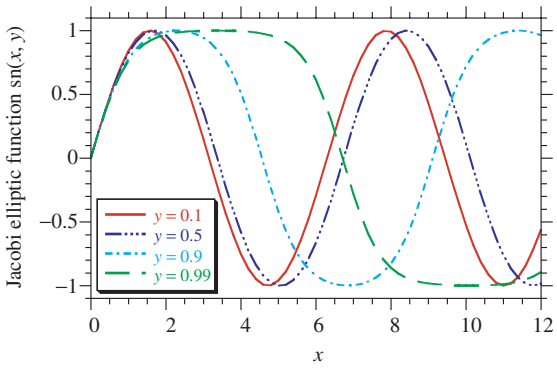


**Figure 8.8** Jacobi elliptic function sn($x$, $y$) vs $x$ for several values of $y$.

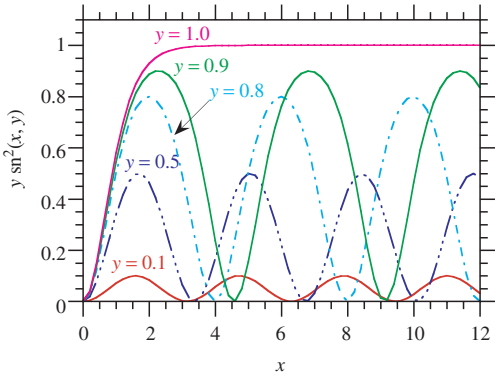


**Figure 8.9** The product $y\ \mathrm{sn}^2(x, y)$ vs $x$ for several values of $y$ models the output of the SFG vs propagation distance in the crystal for various ratios of input field strengths.

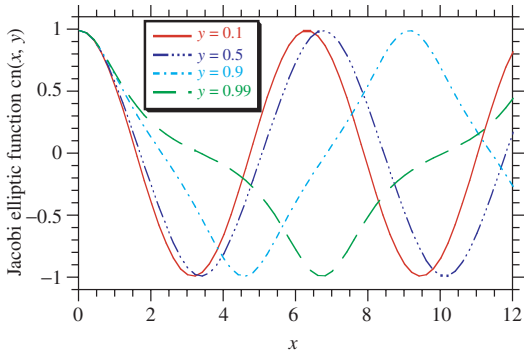


**Figure 8.14** Jacobi elliptic function $\mathrm{cn}(x, y)$ vs $x$ for several values of $y$.

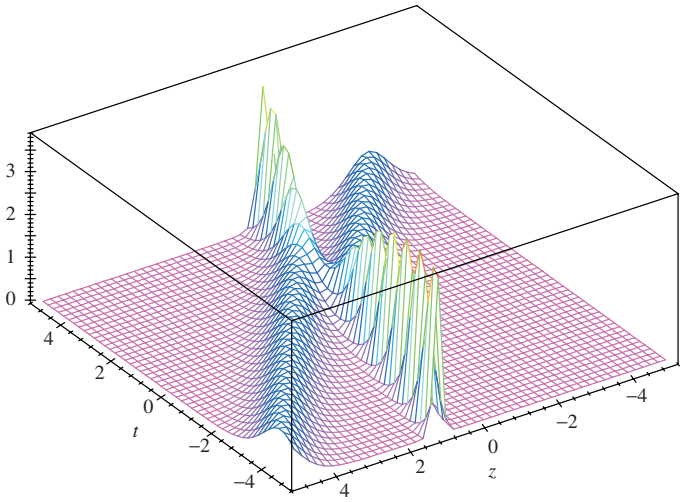


**Figure 8.20** (a) Two-soliton solution for the higher-order NSE, Eq. (8.100). (b) Magnitude of the black soliton $u(z, t)$ in Eq. (8.112) with $B = 1$, and $A = 1.0$, 1.5 and 2.0.